μ^+SR investigation of local magnetic order in $LiCrO_2$

Jun Sugiyama,[1,*] Martin Månsson,[2] Yutaka Ikedo,[1,†] Tatsuo Goko,[3] Kazuhiko Mukai,[1] Daniel Andreica,[4] Alex Amato,[5] Kingo Ariyoshi,[6] and Tsutomu Ohzuku[6]

[1]*Toyota Central Research and Development Laboratories Inc., Nagakute, Aichi 480-1192, Japan*

[2]*Laboratory for Neutron Scattering, ETH Zürich and Paul Scherrer Institut, CH-5232 Villigen PSI, Switzerland*

[3]*TRIUMF, 4004 Wesbrook Mall, Vancouver, British Columbia, Canada V6T 2A3*

[4]*Faculty of Physics, Babes-Bolyai University, 3400 Cluj-Napoca, Romania*

[5]*Laboratory for Muon Spin Spectroscopy, Paul Scherrer Institut, CH-5232 Villigen PSI, Switzerland*

[6]*Department of Applied Chemistry, Graduate School of Engineering, Osaka City University, Osaka 558-8585, Japan*

(Received 2 March 2009; revised manuscript received 6 April 2009; published 8 May 2009)

In order to elucidate the magnetic nature of the lithium chromium dioxide $LiCrO_2$, in which the Cr^{3+} ions form a two-dimensional triangular lattice in the CrO_2 plane, we have performed a positive muon-spin rotation and relaxation (μ^+SR) experiment using a powder sample in the temperature range 1.7–155 K. Weak-transverse-field measurements indicated the existence of a bulk antiferromagnetic (AF) transition at T_N =61.2 K. Below T_N, zero-field (ZF) μ^+SR measurements demonstrated the formation of static long-range order; the observed ZF spectrum was well reproduced by the AF spin structure proposed by neutron measurements. The ZF-μ^+SR measurements also indicated that $LiCrO_2$ is a pure paramagnet for $T \geq 62.5$ K, since its internal magnetic field (H_{int}) can be explained by solely nuclear magnetic moments. This means that, contrary to previous suggestions by susceptibility and heat capacity measurements, no short-range order exists for $T \geq 62.5$ K. However, ZF-μ^+SR detected the change in H_{int} from a low-T static state to a high-T dynamic state at 115 K, most likely connected to a change in the position/motion of the Li ions.

DOI: 10.1103/PhysRevB.79.184411 PACS number(s): 76.75.+i, 75.25.+z, 75.40.Gb

I. INTRODUCTION

In nonbipartite lattices such as the triangular one, in the case of half filling the Hubbard model has an extraordinarily rich ground-state structure including a paramagnetic phase, different long-range orders, and also metal-insulator transitions. Historically the triangular lattice system has served as a playground for new ideas about various unconventional phases of frustrated antiferromagnets.[1]

In this context, the layered cobalt dioxides have been the center of attention for many years.[2,3] The two main driving forces have been the electrochemical importance of the $LiCoO_2$ compound as an electrode in Li-ion batteries,[4] and by the unconventional superconductivity discovered in the $Na_{0.35}CoO_2 \cdot 1.3H_2O$ compound.[5] Further, the layered nickel dioxides, e.g., $LiNiO_2$, and Ag_2NiO_2 have also been subjects of many investigations[6–8] due to a coupling of magnetic properties and intriguing structural phase transitions. However, there have been very limited experimental studies on the layered chromium dioxides,[9–13] such as $LiCrO_2$, $NaCrO_2$, and $KCrO_2$, despite their potential use in rechargeable batteries[14] and as catalysts.[15] Further, most of these studies were performed more than ten years ago. However, very recently, a newfound interest for the layered chromium dioxides has started, as shown by both experimental[16] and theoretical[17] work. In the case of the closely related $AgCrO_2$, the layered chromium dioxides are also found to be of current interest as a multiferroic material.[18]

The crystal structure of $LiCrO_2$ was reported to be an α-$NaFeO_2$-type rhombohedral system of space group $R\bar{3}m$(a_H=2.9010 Å, c_H=14.4311 Å).[19] Here, a_H denotes the a-axis length of the CrO_2 plane in hexagonal setting. In this structure, single CrO_2 sheets and single disordered Li planes form alternating stacks along the hexagonal c axis (see Fig. 1). Its magnetic structure is close to the ideal 120° structure characteristic of the nearest-neighbor Heisenberg model on a two-dimensional triangular lattice (2DTL). The Cr ions are expected to have a valence +3 and to be in a $S = \frac{3}{2}$ spin state, although the valence state of the Cr ions would be affected by structural distortion of the $LiCrO_2$ lattice. For $LiNiO_2$,[6] $NaNiO_2$,[20,21] and $Na_{0.75}CoO_2$,[22,23] an A-type antiferromagnetic (AF) order is present at low T, with ferromagnetic (FM) order within the Ni/Co planes and AF order between the planes. The intraplane FM order naturally comes from superexchange along the 90° O-Ni/Co-O bond angle. The O-Cr-O bond angle is also close to 90°, hence the same intraplane FM order could be expected. However, experimental work regarding $NaCrO_2$ (Ref. 16) and $LiCrO_2$ (Ref. 9), as well as theoretical studies of $LiCrO_2$ (Ref. 17) show, in agreement, that the intraplane magnetic interaction is *strongly* AF, while the interplane is very weak and also AF.

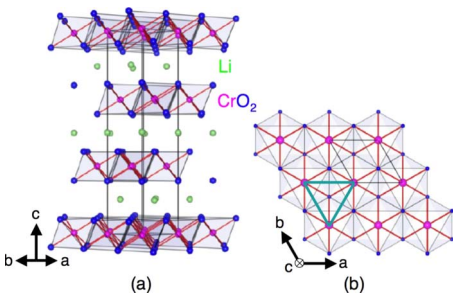

FIG. 1. (Color online) Crystal structure of $LiCrO_2$ showing (a) alternating stacks of Li and CrO_2 layers along the c axis and (b) top view along the c axis demonstrating the triangular configuration of the Cr ions.

The explanation to this difference is to be found in the enhanced direct overlap between the metal d orbitals in layered chromium dioxides. Indeed there exists a driving force toward FM intraplane order through superexchange via the ~94° O-Cr-O bond. However, the large direct $d-d$ overlap of Cr surpasses the superexchange and instead drives the intraplane order to be AF. This has been shown to be true by experimental[9] as well as theoretical[17] work. In addition, it has also been shown that the increased charge-transfer $p-d$ gap reduces the ferromagnetic superexchange in layered chromium dioxides, further strengthening the AF order within the Cr planes.

From susceptibility measurements, electronic paramagnetic resonance, and Mössbauer spectroscopy,[9,24,25] it has been shown that a clear long-range AF order sets in below T_N=62 K. Further, the same bulk susceptibility data show that this compound does not follow Curie-Weiss law below approximately 300 K.[25] This could indicate that a possible short-range order sets in well above T_N and long-range order is finally achieved for $T<T_N$. Some support for this statement could be found in heat capacity (C_p) measurements[25] that shows a contribution to magnetic entropy all the way up to $T=4T_N$. However, to the author's knowledge, there has been no direct experimental evidence of short-range order and in fact no experimental study is to be found in the published literature regarding the microscopic magnetic nature of $LiCrO_2$.

The positive muon-spin rotation and relaxation (μ^+SR) technique has during the last 30 years been established as a unique and powerful method to study local magnetic fields and spin order in a wide range of materials.[26–29] By implanting highly spin polarized muons ($S=\frac{1}{2}$) into a material and monitoring the angular and temporal decay into positrons, the muon acts as a unique and highly *localized* magnetic probe. Contrary to other magnetic resonance techniques (e.g., NMR), μ^+SR is the only technique that can directly probe an internal magnetic field caused by magnetic order/moments without any externally applied field. In this paper, we present a first principal study of microscopic magnetic order and transitions in this 2DTL material using zero-field (ZF) as well as weak transverse-field (wTF) μ^+SR.

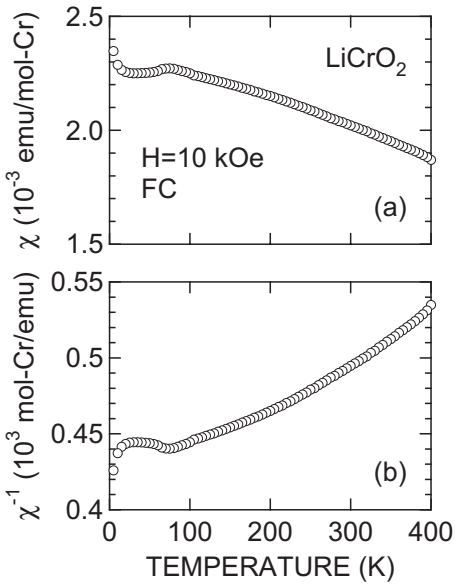

FIG. 2. Temperature dependence of (a) magnetic susceptibility (χ) and (b) inverse χ for the powder sample of $LiCrO_2$. χ was measured in field-cooling (FC) mode with magnetic field H =10 kOe.

II. EXPERIMENTAL DETAILS

A powder sample of $LiCrO_2$ was prepared at Osaka City University by a solid-state reaction technique using reagent grade $LiOH \cdot H_2O$ and Cr_2O_3 powders as starting materials. A mixture of the two powders was heated at 1000 °C for 12 h in an air flow. Powder x-ray diffraction analysis showed that the sample was single phase with a rhombohedral system of space group $R\bar{3}m$; the a_H-axis length was 2.899 Å and the c_H-axis length was 14.418 Å. An inductively coupled plasma analysis indicated that the Li/Cr ratio was 1.03.

The pressed powder was placed in a small envelope made of very thin Al-coated Mylar tape and then attached to a low-background fork-type sample holder. In order to stop the muons primarily inside the sample, we made sure that the side facing the muon beamline was only covered by a single layer of Mylar tape. Subsequently, μ^+SR spectra were measured at the Swiss Muon Source (SμS), Paul Scherrer Institut, Villigen, Switzerland. By using the surface muon beamline μE1 and the Dolly spectrometer, ZF, wTF, and weak longitudinal-field (LF) spectra were collected for 1.7 K$\leq T \leq$155 K. The experimental setup and techniques were described in detail elsewhere.[29]

The magnetic susceptibility (χ) of the sample was measured using a superconducting quantum interference device magnetometer (MPMS, Quantum Design) in the T range between 400 and 5 K under magnetic field $H \leq 10$ kOe. As seen in Fig. 2, $\chi(T)$ data from the present sample reproduce the prior measurements reported in Refs. 9, 12, and 25.

III. EXPERIMENTAL RESULTS

A. Overall feature by wTF-μ^+SR

Figure 3 shows the variation in the wTF time spectra acquired at different temperatures. When T decreases below

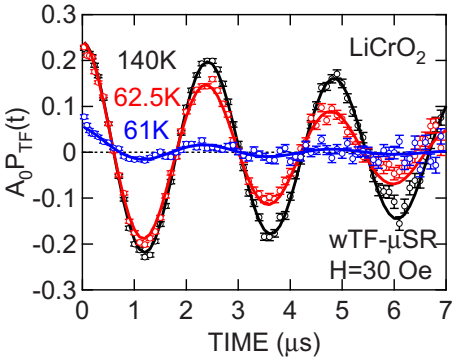

FIG. 3. (Color online) Temperature dependence of the wTF(=30 Oe) μ^+SR time spectra. Solid lines represent the fitting result using Eq. (1).

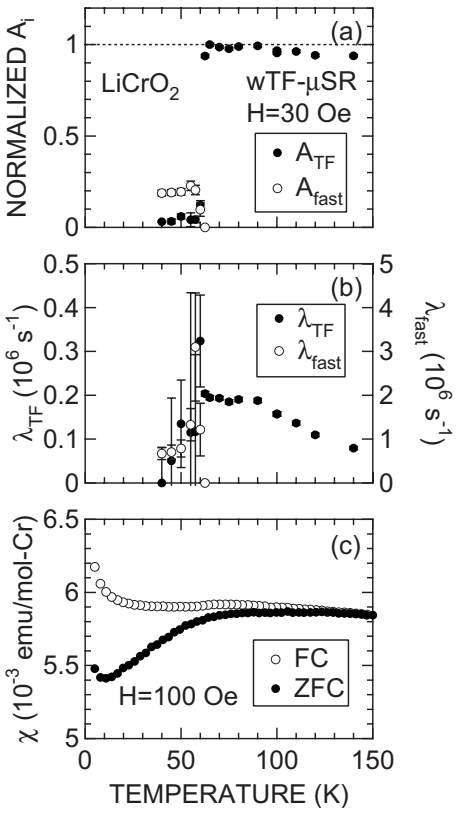

FIG. 4. Temperature dependences of (a) normalized asymmetries (A_{TF} and A_{fast}), (b) exponential relaxation rates (λ_{TF} and λ_{fast}), and (c) magnetic susceptibility (χ). The data in (a) and (b) were obtained by fitting the wTF spectra using Eq. (1). χ was measured both in FC and zero-field-cooling (ZFC) mode with magnetic field $H=100$ Oe.

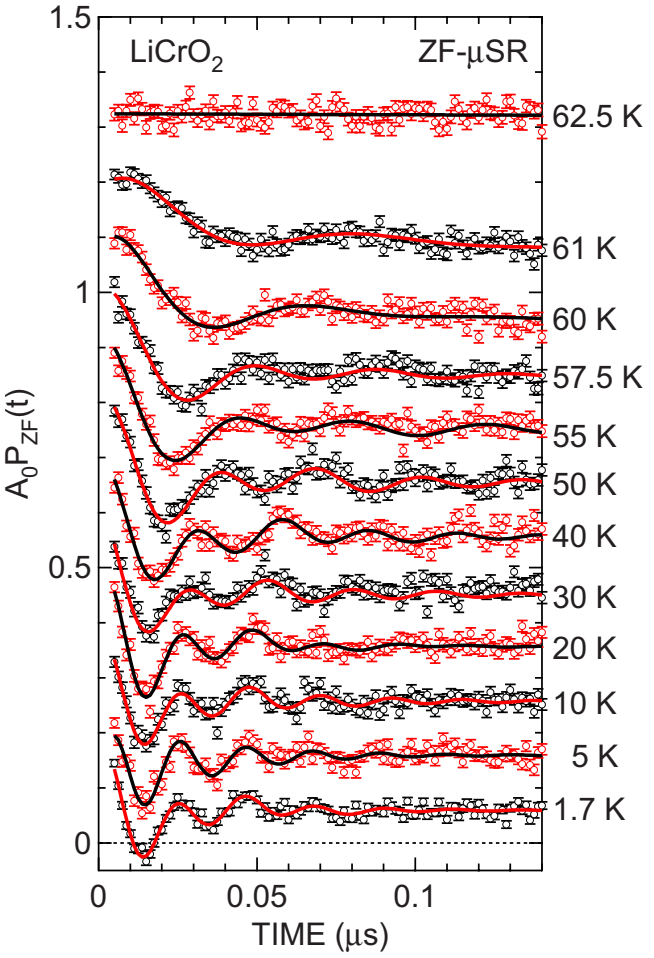

FIG. 5. (Color online) Temperature-dependent ZF-μ^+SR spectra for $LiCrO_2$. Solid lines represent the fitting result using Eq. (2). Each spectrum is offset by 0.1 for clarity of display.

62.5 K, the oscillation amplitude due to wTF rapidly decreases, indicating the appearance of additional strong internal magnetic field(s) (H_{int}). The wTF-μ^+SR spectrum was consequently fitted using a combination of a slowly relaxing precessing signal and a fast relaxing nonoscillatory signal. The first component is due to the externally applied magnetic field (wTF=30 Oe) and the second due to H_{int}:

$$A_0 P_{TF}(t) = A_{TF}\cos(\omega_{TF}^{\mu} t + \phi_{TF})\exp(-\lambda_{TF} t) + A_{fast}\exp(-\lambda_{fast} t), \quad (1)$$

where A_0 is the initial ($t=0$) asymmetry, $P_{TF}(t)$ is the muon spin polarization function, ω_{TF}^{μ} is the muon Larmor frequency corresponding to the applied wTF, ϕ_{TF} is the initial phase of the precessing signal, λ_{TF} and λ_{fast} are the exponential relaxation rates, and A_{TF} and A_{fast} are the asymmetries of the two components of the μ^+SR spectrum. This form was chosen because the externally applied magnetic field is much weaker than the local (internal) magnetic fields in the ordered phase. By plotting A_{TF} versus T [see Fig. 4(a)], we can clearly see that the sample has a bulk magnetic transition at $T_N=61.2$ K, where the normalized $A_{TF}(=A_{TF}/A_0=N_{A_{TF}})=0.5$. This value of T_N is in excellent agreement with the current and past $\chi(T)$ data [see Figs. 2 and 4(c)].

The $\lambda_{TF}(T)$ curve exhibits a slow increase with decreasing T until T_N is reached, although $N_{A_{TF}}\sim 1$ at T above T_N, indicating that the whole volume of the $LiCrO_2$ sample is in a paramagnetic state. This means an evolution of local magnetic inhomogeneity with decreasing T below 140 K. Indeed, since the $\chi_{FC}(T)$ curve starts to deviate from the $\chi_{ZFC}(T)$ curve below $\sim$130 K, the macroscopic magnetic nature is also altered below $\sim$130 K, in spite of the fact that $LiCrO_2$ is paramagnetic down to T_N.

In contrast, since the A_{TF} signal eventually disappears below T_N, it is very difficult to accurately estimate λ_{TF} below T_N. The normalized $A_{fast}(=A_{fast}/A_0=N_{A_{fast}})$ has a nonzero value below T_N and increases with decreasing T, and finally levels off to $\sim$0.2 below 50 K. The fact that $N_{A_{fast}}$ never reaches the full asymmetry (=1) suggests the presence of a fast relaxing/precessing signal in the wTF spectrum. However, in order to distinguish such a signal, the ZF-μ^+SR technique with high statistics is more suitable.

B. ZF-μ^+SR below T_N

In order to demonstrate the formation of static magnetic order below T_N, Fig. 5 shows the T dependence of ZF-μ^+SR

time spectrum in the T range between 1.7 and 62.5 K. Below T_N, muon spins are clearly precessing due to the appearance of a spontaneous $H_{\rm int}$, resulting in a clear oscillation in the ZF-μ^+SR spectrum. The ZF spectrum was well fitted by the combination of two damped cosine oscillations, which are originating from the static ordered $H_{\rm int}$, and a slowly relaxing nonoscillatory signal due to the "1/3 tail" caused by the field components parallel to the initial muon-spin polarization:

$$A_0 P_{\rm ZF}(t) = A_{\rm AF1}\exp(-\lambda_{\rm AF1}t)\cos(\omega^{\mu}_{\rm AF1}t+\phi_1) + A_{\rm AF2} \times\exp(-\lambda_{\rm AF2}t)\cos(\omega^{\mu}_{\rm AF2}t+\phi_2) + A_{\rm tail}\exp(-\lambda_{\rm tail}t). \quad (2)$$

Here, A_0 is the initial ($t=0$) asymmetry, $P_{\rm ZF}(t)$ is the muon-spin polarization function in ZF, $\omega^{\mu}_{\rm AF1}$ and $\omega^{\mu}_{\rm AF2}$ are the two muon Larmor frequencies corresponding to the ordered $H_{\rm int}$'s, ϕ_1 and ϕ_2 are the initial phases of the precessing signals, $\lambda_{\rm AF1}$ and $\lambda_{\rm AF2}$ are the exponential relaxation rates of the precessing signals, $\lambda_{\rm tail}$ is the exponential relaxation rate of the tail signal, and $A_{\rm AF1}$, $A_{\rm AF2}$, and $A_{\rm tail}$ are the asymmetries of the three signals.

The fit for the ZF spectrum at the lowest T measured (1.7 K) yields $\phi_1=48\pm6°$ and $\phi_2=-52\pm7°$. This indicates that, although Eq. (2) well reproduces the obtained ZF spectrum as seen in Fig. 5, it is too simple for describing $H_{\rm int}$ in the AF ordered state. In other words, this implies the formation of a complex AF structure, as in the case for NaV_2O_4 (Ref. 30), because ϕ_i should be zero for a simple commensurate AF order. Indeed, neutron measurements proposed a double-Q 120° structure[12] with two different wave numbers $q=(\frac{1}{3},\frac{1}{3},0)$ and $(-\frac{2}{3},\frac{1}{3},\frac{1}{2})$. This means the presence of a wide distribution of $H_{\rm int}$ at the muon sites (see Sec. IV A). However, since the determined AF spin structure is commensurate to the lattice, it is reasonable to fix $\phi_1=\phi_2=0$. Actually, when we use a common $\phi(=\phi_1=\phi_2)$ in Eq. (2), we obtain $\phi=-8\pm3°$ (eventually 0), as expected. The other μ^+SR parameters at 1.7 K, when we fix $\phi_1=\phi_2=0$, are obtained as $A_{\rm AF1}=0.108\pm0.002$, $A_{\rm AF2}=0.073\pm0.002$, $A_{\rm tail}=0.059$, $f_{\rm AF1}=\omega^{\mu}_{\rm AF1}/2\pi=24.3\pm0.6$ MHz, $f_{\rm AF2}=\omega^{\mu}_{\rm AF2}/2\pi=41.9\pm0.3$ MHz, $\lambda_{\rm AF1}=(52\pm3)\times10^6$ s^{-1}, $\lambda_{\rm AF2}=(30\pm2)\times10^6$ s^{-1}, and $\lambda_{\rm tail}=(0.037\pm0.002)\times10^6$ s^{-1}. Note that we fixed the total asymmetry as 0.24, i.e., $A_{\rm AF1}+A_{\rm AF2}+A_{\rm tail}=0.24$. Since the preliminary fit at each T indicated that $A_{\rm AF1}$, $A_{\rm AF2}$, $A_{\rm tail}$, and ϕ was almost T independent except below the vicinity of T_N, we attempted to fit all the ZF spectra below T_N using common $A_{\rm AF1}$, $A_{\rm AF2}$, $A_{\rm tail}$, and $\phi=0$, i.e., a *global fit* technique.

Figure 6 shows the T dependences of the μ^+SR parameters obtained by a *global fit* with common $A_{\rm AF1}=0.10678\pm0.00013$, $A_{\rm AF2}=0.07424\pm0.00013$, $A_{\rm tail}=0.05898$. Here $A_{\rm tail}$ is approximately only 3/4 of the expected value for the tail (0.24/3), most probably due to preferred orientation caused by pressing of the $LiCrO_2$ powder. Making comparison with the result of the wTF measurements, $A_{\rm tail}$ is almost equivalent to $A_{\rm fast}$, which should correspond to the 1/3 tail. This clearly supports the above assignment for the $A_{\rm tail}$ signal.

The two $f_{{\rm AF}i}(T)$ curves exhibit an order-parameter-like T dependence, although it is difficult to evaluate a critical exponent [β for $f/f_{T\to0\ {\rm K}}=(1-T_N/T)^{\beta}$] due to a lack of data points just below T_N. As T increases from 1.7 K, the two $f_{{\rm AF}i}$'s seem to disappear simultaneously at T_N. This clearly suggests that the two $f_{{\rm AF}i}$'s are not caused by the coexistence of two different phases in the sample but rather by two magnetically inequivalent muon sites in the lattice (see Sec. IV A).

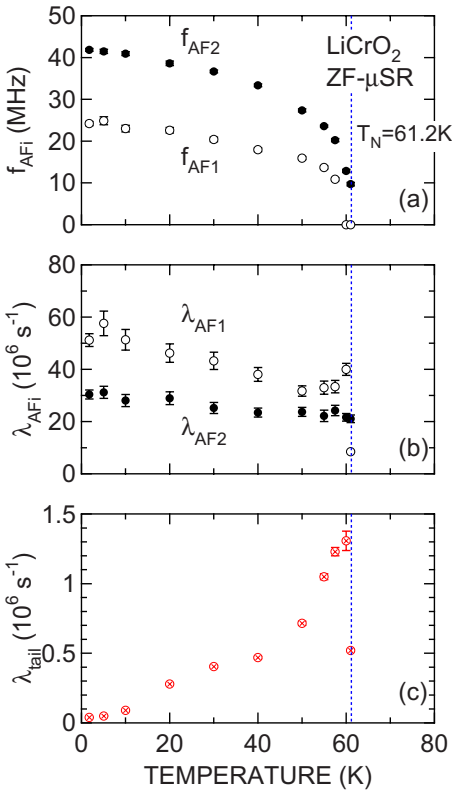

FIG. 6. (Color online) Temperature dependences of (a) muon precession frequencies $f_{\rm AF1}(=\omega^{\mu}_{\rm AF1}/2\pi)$ and $f_{\rm AF2}(=\omega^{\mu}_{\rm AF2}/2\pi)$, (b) exponential relaxation rates ($\lambda_{\rm AF1}$ and $\lambda_{\rm AF2}$), and (c) $\lambda_{\rm tail}$. The data were obtained by *global* fitting of all the ZF spectra using Eq. (2), with common $A_{\rm AF1}(=0.10678)$, $A_{\rm AF2}(=0.07424)$, $A_{\rm tail}(=0.05898)$, and $\phi_1=\phi_2=0$.

The $\lambda_{\rm AF1}$ decreases slowly with increasing T, but increases again below the vicinity of T_N, indicating an increase toward a wider field distribution near T_N. As a result, it is difficult to obtain accurate $f_{\rm AF1}$ in the T range between 60 and T_N. In contrast, the $\lambda_{\rm AF2}(T)$ curve is almost T independent up to T_N. Finally, the magnitude of $\lambda_{\rm tail}$ remains below 1.4×10^6 s^{-1} in the whole T range measured. Although $\lambda_{\rm tail}$ increases with T, its value is 2 orders of magnitude smaller than $\lambda_{\rm AF1}$ and $\lambda_{\rm AF2}$. Furthermore, $\lambda_{\rm tail}$ approaches 0, when $T\to0$. Therefore, it is very reasonable to assign this signal as a 1/3 tail signal.

C. ZF-μ^+SR above T_N

The ZF spectrum exhibits a Kubo-Toyabe behavior just above T_N [see Fig. 7(a)]. This means that the implanted muons *see* the internal magnetic field ($H_{\rm int}$) only due to the nuclear magnetic moments of ^{7}Li and ^{6}Li, together with a minor contribution from ^{53}Cr. Contrary to previous

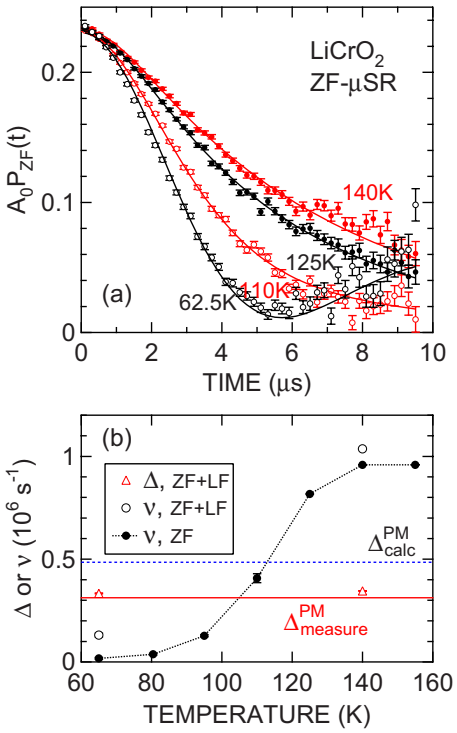

FIG. 7. (Color online) Temperature dependences of (a) ZF-μ^+SR spectrum above T_N and (b) the field distribution width (Δ) shown as triangles and field fluctuation rate (ν) as circles. The data in (b) were obtained by fitting the μ^+SR time spectra to Eq. (3). Closed symbols are obtained from a *global* fit to ZF spectra only, while open symbols are obtained from a *global* fit to both ZF and longitudinal field (LF=20 Oe) spectra at 65 and 140 K. The solid horizontal line in (b) represents a common $\Delta^{\mathrm{PM}}_{\mathrm{measure}}$(=0.3124 $\times 10^6$ s^{-1}) for a global fit, while the dashed horizontal line shows a prediction from dipole field calculations $\Delta^{\mathrm{PM}}_{\mathrm{calc}}$. Dotted curve serves as a guide for the eyes.

suggestions,[25] this finding excludes the possibility of the formation of any short-range order above T_N. In other words, the AF transition is very sharp and continuous, as expected. However, as T increases from 80 K, the minimum in the ZF spectrum ($\sim$6 μs at 80 K) shifts toward a later time domain and the relaxation rate decreases with T. This implies that H_{int} starts to fluctuate above 80 K. Indeed, the ZF spectrum is well fitted by a dynamic Gaussian Kubo-Toyabe function $[G^{\mathrm{DGKT}}(\Delta,\nu,t)]$ for H_{int} due to the fluctuating nuclear magnetic moments;

$$A_0 P_{\mathrm{ZF}}(t) = A_{\mathrm{KT}} G^{\mathrm{DGKT}}(\Delta,\nu,t), \tag{3}$$

where Δ is the static width of the local frequency at the disordered sites, and ν is the field fluctuation rate. A preliminary fit using Eq. (3) for the ZF spectrum at each T between 62.5 and 155 K indicated that the two parameters, A_{KT} and Δ, are approximately independent of T. All of the ZF spectra were, therefore, fitted by Eq. (3) using common A_{KT} and Δ. The global fit provides that $A_{\mathrm{KT}}=0.2309\pm0.0002$ and $\Delta=(0.3124\pm0.0001)\times10^6$ s^{-1}.

Figure 7(b) shows the T dependence of ν for $LiCrO_2$ together with the T-independent $\Delta^{\mathrm{PM}}_{\mathrm{measure}}$. The $\nu(T)$ curve shows a *dull* but steplike change from almost 0 to $\sim$0.96 $\times 10^6$ s^{-1} in the T range between 80 and 140 K. This demonstrates the appearance of dynamical fluctuation of H_{int} above $\sim$80 K. In addition, weak longitudinal field (LF =20 Oe) measurements at 65 and 140 K supports the $\nu(T)$ and $\Delta(T)$ curve obtained by the global fit for the ZF spectra. Moreover, the $\chi_{\mathrm{FC}}(T)$ curve starts to deviate from the $\chi_{\mathrm{ZFC}}(T)$ curve below approximately 130 K [see Fig. 4(c)]. This evidences the intrinsic change in a magnetic environment of $LiCrO_2$ around 130 K. Therefore, it is very reasonable to consider the change in Li motion/position as an origin of the increase in ν above 80 K. The detail of the T dependence of ν will be discussed in Sec. IV B.

IV. DISCUSSION

A. Muon sites and H_{int}

According to electrostatic potential calculations, positive muons are most likely to locate in the vicinity of the O^{2-} ions; that is, $\sim$1 Å away from the O^{2-} ions along the c axis. Further, assuming the AF spin structure, i.e., the double-Q 120° structure, proposed by neutron measurements,[12] there exist 36 magnetically different muon sites, although there is crystallographically only one muon site in the $LiCrO_2$ lattice. This is because the magnetic unit cell is reported to be three times larger than the crystallographic unit cell. Also, due to the helical spin structure along the c axis, the muon site above a certain O^{2-} ion is magnetically different from that below the O^{2-} ion. Since there are 6 oxygen in the crystallographic unit cell for Z=3, the total number of the muon sites is provided by $6\times2\times3=36$.

Dipole field calculations for the 36 muon sites yielded a field distribution shown in Fig. 8(a) at the muon sites for the AF ordered state. The ZF-μ^+SR time spectrum is thus given by

$$P_{\mathrm{ZF}}(t) = \frac{2}{3}\frac{1}{36}\sum_{i=1}^{36}\cos(2\pi f_i t)\exp(-\lambda_i t) + \frac{1}{3}, \tag{4}$$

where f_i and λ_i are the muon precession frequency and its exponential relaxation rate, respectively, at the ith site ($f_i < f_{i+1}$). Here, f_i is converted into $H_{\mathrm{int},i}$ by $f_i = 13.553$ kHz/Oe$\times H_{\mathrm{int},i}$. When $\lambda_i=0$, we obtain the ZF spectrum without relaxation, as seen in Fig. 8(b). Then, the calculated ZF spectrum was fitted by Eq. (2). As seen in Table I, such fit reproduces a delay and progress of ϕ_i, obtained by the fit for the measured spectrum at 1.7 K. This clearly demonstrates that the delay and progress of ϕ_i are caused by a wide field distribution and also confirms the reliability of the proposed AF spin structure and the dipole field calculations. Moreover, since the fit by Eq. (2) with $\phi_i=0$ yields a very similar result to that obtained by Eq. (2), the result of the *global fit* is acceptable.

Even for the calculated spectrum without a relaxation, the fit using Eq. (2) provides that $\lambda_{\mathrm{AF1}}=(38\pm9)\times10^6$ s^{-1} and $\lambda_{\mathrm{AF2}}=(1\pm2)\times10^6$ s^{-1}. Since we measured a powder sample, a random distribution of H_{int} together with an imperfection of the crystalline solid naturally induce an additional relaxation. Also, even for single crystal samples, the ordered

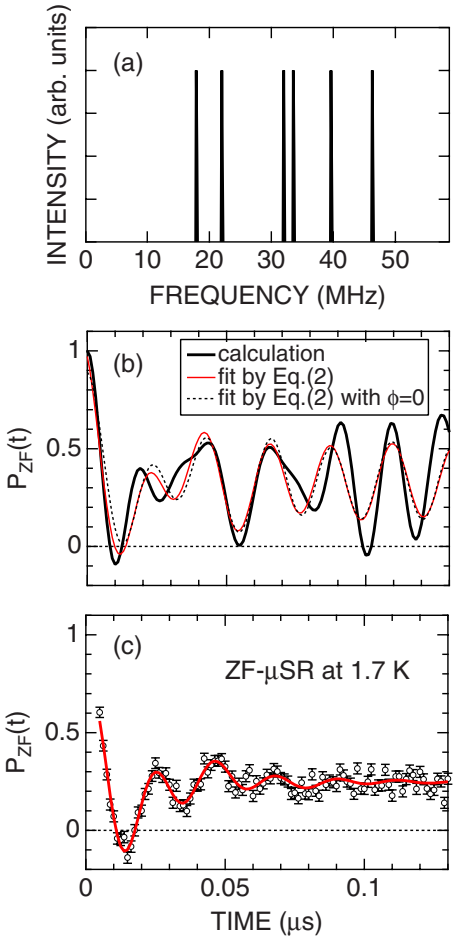

FIG. 8. (Color online) (a) Field distribution for $LiCrO_2$ predicted from dipole field calculations (vertical bars) using the spin structure from Ref. 12, (b) calculated ZF-μ^+SR time spectrum (thick solid line) and the fit curve using Eq. (2) (thin solid line) and Eq. (2) with $\phi_i=0$ (thin broken line), and (c) measured ZF-μ^+SR time spectrum at 1.7 K. In the calculations, we used $\mu_{ord}=2.7\ \mu_B$, where μ_{ord} is the magnitude of the ordered moment of the Cr ions estimated by neutron measurements (Ref. 12). The calculated ZF spectrum was obtained by Eq. (4) with $\lambda_i=0$.

spin lattice is not perfect to the implanted muons causing a nonzero relaxation rate in the ZF spectrum.[29] We wish to note that the prediction for the magnitude of $\lambda_{AF,i}$ (i.e., $\lambda_{AF1}>\lambda_{AF2}$) is consistent with the fit result for the ZF spectrum measured at 1.7 K.

The calculated f_i is proportional to the AF ordered moment (μ_{ord}) of the Cr ions. Since μ_{ord} is reported 2.7 μ_B at 9 K for the double-Q 120° structure by the neutron experiment,[12] we used $\mu_{ord}=2.7\ \mu_B$ for the present dipole field calculations. Figure 8 shows that the calculated spectrum roughly reproduces the measured ZF spectrum if we ignore damping. More correctly, based on the fit result of $f_{AF,i}$ in Table I, μ_{ord} is estimated as $2.4\pm0.1\ \mu_B$ from the present μ^+SR measurements, being consistent with the neutron results.

Taking into account the nuclear magnetic moments of ^{7}Li, ^{6}Li, and ^{53}Cr, the same dipole field calculations in the paramagnetic state provided that $\Delta_{calc}^{PM}=(0.485\pm0.002)\times10^6\ s^{-1}$. This is roughly in agreement with the experimental result, although the calculated Δ_{calc}^{PM} is 55% larger [see Fig. 7(b)] than the measured $\Delta_{measure}^{PM}$[$=(0.3124\pm0.0001)\times10^6\ s^{-1}$]. Consequently, the muon sites, which are predicted by the electrostatic potential calculations, are found to give reasonable H_{int} both for the AF ordered state and the paramagnetic state.

B. Possible origin of the anomaly around 115 K

The $\nu(T)$ curve demonstrates a clear change of H_{int} from a low-T static state to a high-T dynamic state at $T_c\sim115$ K, at which $\nu=\frac{1}{2}[\nu(65\ K)+\nu(155\ K)]$. Since ν appears to level off to a constant value above 140 K [see dotted curve in Fig. 7(b)], the change at T_c is most unlikely due to a diffusive motion of the Li^+ ions. This is because the relationship between ν and T is expected to be given by $\nu\propto\exp(-1/T)$ for Li diffusion.[31] Therefore, T_c is more likely to be associate with a structural transition caused by the change in the position of Li^+ ions. In other words, T_c could be explained by an order-disorder transition of the Li^+ ions; i.e., the Li ions could slightly shift their position from the regular site at low T. Moreover, Δ is expected to be insensitive to such small displacement of the Li^+ ions, when the Li^+ ions locate in the vicinity of the regular Li site.

Such transition would induce a charge disproportionation of the Cr ions; i.e., $Cr^{3+}\rightarrow Cr^{3+\delta}+Cr^{3-\delta}$, as in the case for $Na_{0.5}CoO_2$.[32,33] However, even for the mixed valence state of the Co ions in $Na_{0.5}CoO_2$, δ was reported below 0.2.[32,33] Hence, it would be very difficult to detect δ for $LiCrO_2$, even if such charge disproportionation occurs. Actually, although we attempted to fit the ZF spectrum by $G^{DGKT}(\Delta,\nu,t)\exp(-\lambda_{Cr}t)$, where the exponential relaxation should corre-

TABLE I. Fit parameters obtained by Eq. (2) for the calculated and measured spectrum.

Calculated spectrum	A_{AF1}/A_{AF2}	f_{AF1} (MHz)	f_{AF2} (MHz)	λ_{AF1} ($10^6\ s^{-1}$)	λ_{AF2} ($10^6\ s^{-1}$)	ϕ_1 (deg)	ϕ_2 (deg)
Equation (2)	2.4 ± 1.0	25.8 ± 1.3	45.1 ± 0.3	38 ± 9	1 ± 2	44.4 ± 0.2	-49.9 ± 0.2
Equation (2) with $\phi_i=0$	1.7 ± 0.7	27.8 ± 0.9	45.7 ± 0.2	31 ± 8	1 ± 2	0	0
Measured spectrum at 1.7 K							
Equation (2)	1.16 ± 0.05	17.3 ± 0.9	45.8 ± 0.6	52 ± 4	34 ± 2	48 ± 7	-52 ± 7
Equation (2) with $\phi_i=0$	1.48 ± 0.07	24.3 ± 0.6	41.9 ± 0.3	52 ± 3	30 ± 2	0	0

spond to the fluctuation of the Cr spins, the $\lambda_{Cr}(T)$ curve exhibits no crucial anomaly around T_c. It should also be noted that a Kubo-Toyabe function is only an *approximation of the nuclear dipole contribution* to the ZF-μ^+SR spectrum. Hence, although the spectrum is well fitted by a Kubo-Toyabe function, there is still a possibility that the dynamics observed above T_N originates from electronic moments. In order to further investigate the details of this transition, we need to measure the ZF and LF spectra at high T using a pulse-muon facility, such as, ISIS in the U.K. or J-PARC in Japan. Furthermore, it is more preferable to perform a precise structural analysis of $LiCrO_2$ as a function of T by both neutron and x-ray (from a synchrotron radiation source) diffraction.

Finally, we wish to address the possible role of the order-disorder transition of the Li ions for the magnetic nature of $LiCrO_2$. In contrast to $NaCrO_2$, for which no long-range AF order is observed by neutron measurements down to the lowest T measured,[10,34] a long-range AF order is clearly detected in $LiCrO_2$ by neutron measurements,[12] for reasons currently unknown. As in the case for $Na_{0.5}CoO_2$ (Refs. 35 and 36) and $K_{0.5}CoO_2$,[37,38] the Li ordering in $LiCrO_2$ below 115 K is expected to alter the charge distribution within the CrO_2 planes, and could hereby stabilize the long-range order below T_N. Also, since the Kubo-Toyabe behavior is observed for $T \geq 62.5$ K, it is most unlikely that (previously suggested) short-range order is present above T_N in $LiCrO_2$. In order to explain non Curie-Weiss behavior of the $\chi(T)$ curve at high T, we thus need another mechanisms such as a Li disordering above 115 K inducing slight delocalization of the charge/spin state of the Cr ions, resulting in the difference between the $\chi_{FC}(T)$ and $\chi_{ZFC}(T)$ curve below 130 K. Also, such Li disordering would provide an additional contribution to C_p, which is probably difficult to distinguish from a magnetic contribution by only subtracting C_p for $LiCoO_2$ from C_p for $LiCrO_2$,[25] as in the case for $Na_{0.62}CoO_2$.[39]

V. CONCLUSIONS

By means of a positive muon-spin rotation and relaxation (μ^+SR) technique, we have clarified the magnetic nature of $LiCrO_2$, in which the Cr^{3+} ions form a two-dimensional triangular lattice in the CrO_2 plane. Below $T_N = 61.2$ K, ZF-μ^+SR measurements demonstrate the formation of static AF order. The observed ZF spectrum was well explained by the AF spin structure proposed by neutron measurements. Furthermore, the ZF-μ^+SR measurements clearly indicated the absence of magnetic order for $T \geq 62.5$ K, whether it is long ranged or short ranged. Instead, a dynamic change in the Li motion was detected at approximately $T = 115$ K, probably due to an order-disorder transition within the Li planes.

ACKNOWLEDGMENTS

This work was performed at the Swiss Muon Source, Paul Scherrer Institut, Villigen, Switzerland and we are thankful to Robert Scheuermann for assistance with the μ^+SR experiments. Y.I. and J.S. were partially supported by the KEK-MSL Inter-University Program for Overseas Muon Facilities. This work was also supported by Grant-in-Aid for Scientific Research (B), Grant No. 19340107, MEXT, Japan. All images involving crystal structure were made with VESTA.

*e0589@mosk.tytlabs.co.jp

†Present address: Muon Science Laboratory, Institute of Materials Structure Science, KEK, 1-1 Oho, Tsukuba, Ibaraki 305-0801, Japan.

[1] P. W. Anderson, Mater. Res. Bull. **8**, 153 (1973).

[2] J. Sugiyama, J. H. Brewer, E. J. Ansaldo, H. Itahara, T. Tani, M. Mikami, Y. Mori, T. Sasaki, S. Hébert, and A. Maignan, Phys. Rev. Lett. **92**, 017602 (2004).

[3] K. Mukai, Y. Ikedo, H. Nozaki, J. Sugiyama, K. Nishiyama, D. Andreica, A. Amato, P. L. Russo, E. J. Ansaldo, J. H. Brewer, K. H. Chow, K. Ariyoshi, and T. Ohzuku, Phys. Rev. Lett. **99**, 087601 (2007).

[4] K. Mizushima, P. C. Jones, P. J. Wiseman, and J. B. Goodenough, Mater. Res. Bull. **15**, 783 (1980).

[5] K. Takada, H. Sakurai, E. Takayama-Muromachi, F. Izumi, R. A. Dilanian, and T. Sasaki, Nature (London) **422**, 53 (2003).

[6] J. Sugiyama, K. Mukai, Y. Ikedo, P. L. Russo, H. Nozaki, D. Andreica, A. Amato, K. Ariyoshi, and T. Ohzuku, Phys. Rev. B **78**, 144412 (2008).

[7] J. Sugiyama, Y. Ikedo, K. Mukai, J. H. Brewer, E. J. Ansaldo, G. D. Morris, K. H. Chow, H. Yoshida, and Z. Hiroi, Phys. Rev. B **73**, 224437 (2006).

[8] H. Nozaki, J. Sugiyama, M. Janoschek, B. Roessli, V. Pomjakushin, L. Keller, H. Yoshida, and Z. Hiroi, J. Phys.: Condens. Matter **20**, 104236 (2008).

[9] C. Delmas, G. Le Flem, C. Fouassier, and P. Hagenmuller, J. Phys. Chem. Solids **39**, 55 (1978).

[10] J. L. Soubeyroux, D. Fruchart, C. Delmas, and G. Le Flem, J. Magn. Magn. Mater. **14**, 159 (1979).

[11] S. Angelov, J. Darriet, C. Delmas, and G. Le Flem, Solid State Commun. **50**, 345 (1984).

[12] H. Kadowaki, H. Takei, and K. Motoya, J. Phys.: Condens. Matter **7**, 6869 (1995).

[13] V. R. Galakhov, E. Z. Kurmaev, St. Uhlenbrock, M. Neumann, D. G. Kellerman, and V. S. Gorshkov, Solid State Commun. **95**, 347 (1995).

[14] K.-S. Kim, S.-W. Lee, H.-S. Moon, H.-J. Kim, B.-W. Cho, W.-I. Cho, J.-B. Choi, and J.-W. Park, J. Power Sources **129**, 319 (2004).

[15] E. Cauda, D. Mescia, D. Fino, G. Saracco, and V. Specchia, Ind. Eng. Chem. Res. **44**, 9549 (2005).

[16] A. Olariu, P. Mendels, F. Bert, B. G. Ueland, P. Schiffer, R. F. Berger, and R. J. Cava, Phys. Rev. Lett. **97**, 167203 (2006).

[17] I. I. Mazin, Phys. Rev. B **75**, 094407 (2007).

[18] S. Seki, Y. Onose, and Y. Tokura, Phys. Rev. Lett. **101**, 067204 (2008).

[19] A. Tauber, W. M. Moller, and E. Banks, J. Solid State Chem. **4**, 138 (1972).

[20] C. Darie, P. Bordet, S. de Brion, M. Holzapfel, O. Isnard, A. Lecchi, J. E. Lorenzo, and E. Suard, Eur. Phys. J. B **43**, 159 (2005).
[21] M. J. Lewis, B. D. Gaulin, L. Filion, C. Kallin, A. J. Berlinsky, H. A. Dabkowska, Y. Qiu, and J. R. D. Copley, Phys. Rev. B **72**, 014408 (2005).
[22] S. P. Bayrakci, I. Mirebeau, P. Bourges, Y. Sidis, M. Enderle, J. Mesot, D. P. Chen, C. T. Lin, and B. Keimer, Phys. Rev. Lett. **94**, 157205 (2005).
[23] L. M. Helme, A. T. Boothroyd, R. Coldea, D. Prabhakaran, D. A. Tennant, A. Hiess, and J. Kulda, Phys. Rev. Lett. **94**, 157206 (2005).
[24] N. O. Moreno, C. Israel, P. G. Pagliuso, A. J. Garcia-Adeva, C. Rettori, J. L. Sarrao, J. D. Thompson, and S. B. Oseroff, J. Magn. Magn. Mater. **272-276**, e1023 (2004).
[25] L. K. Alexander, N. Buttgen, R. Nath, A. V. Mahajan, and A. Loidl, Phys. Rev. B **76**, 064429 (2007).
[26] A. B. Denison, H. Graf, W. Kündig, and P. F. Meier, Helv. Phys. Acta **52**, 460 (1979).
[27] S. F. J. Cox, J. Phys. C **20**, 3187 (1987).
[28] P. Dalmas de Réotier and A. Yaouanc, J. Phys.: Condens. Matter **9**, 9113 (1997).
[29] G. M. Kalvius, D. R. Noakes, and O. Hartmann, in *Handbook on the Physics and Chemistry of Rare Earths*, edited by K. A. Gschneidner, Jr., L. Eyring, and G. H. Lander (North-Holland, Amsterdam, 2001), Vol. 32, Chap. 206.
[30] J. Sugiyama, Y. Ikedo, T. Goko, E. J. Ansaldo, J. H. Brewer, P. L. Russo, K. H. Chow, and H. Sakurai, Phys. Rev. B **78**, 224406 (2008).
[31] R. J. Borg and G. J. Dienes, *An Introduction to Solid State Diffusion* (Academic Press, San Diego, 1988).
[32] G. Gasparovic, R. A. Ott, J. H. Cho, F. C. Chou, Y. Chu, J. W. Lynn, and Y. S. Lee, Phys. Rev. Lett. **96**, 046403 (2006).
[33] J. Bobroff, G. Lang, H. Alloul, N. Blanchard, and G. Collin, Phys. Rev. Lett. **96**, 107201 (2006).
[34] D. Hsieh, D. Qian, R. F. Berger, R. J. Cava, J. W. Lynn, Q. Huang, and M. Z. Hasan, J. Phys. Chem. Solids **69**, 3174 (2008).
[35] L. Viciu, J. W. G. Bos, H. W. Zandbergen, Q. Huang, M. L. Foo, S. Ishiwata, A. P. Ramirez, M. Lee, N. P. Ong, and R. J. Cava, Phys. Rev. B **73**, 174104 (2006).
[36] H. W. Zandbergen, M. L. Foo, Q. Xu, V. Kumar, and R. J. Cava, Phys. Rev. B **70**, 024101 (2004).
[37] H. Watanabe, Y. Mori, M. Yokoi, T. Moyoshi, M. Soda, Y. Yasui, Y. Kobayashi, M. Sato, N. Igawa, and K. Kakurai, J. Phys. Soc. Jpn. **75**, 034716 (2006).
[38] Q. Huang, M. L. Foo, J. W. Lynn, H. W. Zandbergen, G. Lawes, Y. Wang, B. H. Toby, A. P. Ramirez, N. P. Ong, and R. J. Cava, J. Phys.: Condens. Matter **16**, 5803 (2004).
[39] M. Blangero, D. Carlier, M. Pollet, J. Darriet, C. Delmas, and J. P. Doumerc, Phys. Rev. B **77**, 184116 (2008).